A New Approach to Compute the Non-Linear Whipping Response Using Hydro-Elastoplastic Coupling

George Jagite, Herve Le Sourne, Patrice Cartraud, Šime Malenica, Fabien Bigot, Jérôme de Lauzon, Quentin Derbanne

A NEW APPROACH TO COMPUTE THE NON-LINEAR WHIPPING RESPONSE USING HYDRO-ELASTOPLASTIC COUPLING

George Jagite*, Hervé le Sourne, Patrice Cartraud
GeM Institute UMR 6183 CNRS
Ecole Centrale Nantes
Nantes, 44300, France
Email: george.jagite@ec-nantes.fr

Šime Malenica, Fabien Bigot, Jérôme de Lauzon, Quentin Derbanne
Research Department
Bureau Veritas
Puteaux, 92800, France

ABSTRACT

In the last ten years, the importance of whipping on the extreme hull girder loads has received much attention, but its consequence on the hull girder's collapse is still unclear. The most common practice is to consider the structural behavior as linear-elastic in the hydro-elastic coupling, and as non-linear elasto-plastic in the ultimate strength evaluation. In order to investigate the influence of the non-linear structural behavior on the hydro-structure interaction responses, a new hydro-elastoplastic model is proposed to compute the non-linear whipping response. The structural part is modeled as two beams connected by a non-linear hinge, which follows the collapse behavior of a ship's hull girder. The hydrodynamic problem is solved using the three-dimensional boundary element method, and the exact coupling between the structural model and the hydrodynamic one is made by making use of the shape function approach. Finally, the fully-coupled hydro-elastoplastic problem is solved directly in time-domain by numerical integration.

INTRODUCTION

The modern world is driven by the need for safe, environmentally friendly, and economic ship designs; in consequence, the prediction of wave-induced motions and loads is of paramount importance. If the structural deformation is negligible during the determination of hydrodynamic responses for the design of rigid ships, in the case of relatively flexible structures (ULCS, VLFS, etc.) the structural and hydrodynamic problems cannot be treated separately, and the two problems must be coupled to account for the wave radiation in the analysis of the structural modes. Henceforth, the evaluation of the wave-induced structural loads for a flexible ship becomes a hydro-structure interaction problem. In other words, the pressures acting on the hull are inducing dynamic loads, and as a result, the response of the structure disturbs the pressure field around the hull.

The preliminary investigations by Bishop and Price [1] fostered an understanding of the physical phenomena behind the hydro-elasticity of ships. Since then, several more or less sophisticated models were proposed, where the hydro-elastic problem is solved at different levels of complexity and accuracy. A comprehensive review of research in the field of hydro-elasticity can be found in [2–4]. Some of the well-established methods based on the potential flow theory are the ones proposed by Tuitman and Malenica [5], and by Kim et al. [6]. Nevertheless, the CFD techniques have evolved significantly in the past decade. Seng [7] developed a numerical method for computing the springing and slamming-induced whipping responses of a ship using OpenFoam. More recent work by Takami and Iijima [8] investigated the combined global and local hydro-elastic response in a large container ship based on two-way coupled CFD and FEA. However, the cost of running a two-way strongly coupled simulation is very high.

Hitherto, it is fair to say that the fully consistent non-linear

*Address all correspondence to this author.

hydro-structure calculations are not practically possible, mainly because both fluid and structure models include transient terms. This kind of complex calculations pose a certain difficulty for the mathematical model, but also the computational complexities can become extremely expensive in terms of computational time and engineering effort.

Notwithstanding the constant improvements in solving the hydrodynamic part of the problem more efficiently and accurately, the structural component is still treated as linear and elastic. After the two accidents: MSC Napoli and MOL Comfort [9, 10], the importance of whipping on the extreme hull girder loads has received much attention, but its consequence on the hull girder's collapse is still unclear. It is worth mentioning that in reality, the collapse behavior is not resulting from the imposed forces, nor displacements (rotations). Instead, it results from the interaction between the collapsing structure and the loads acting on the structure, as pointed out by Lehmann [11]. Thus, there is a need for hydro-elastoplastic models in order to assess the influence of geometric non-linearities, as well as the material non-linearities over the hydrodynamic loads acting on the structure.

With regard to the hydro-elastoplastic behavior, Iijima et al. [12] developed a numerical model in order to follow the collapse behavior of a ship's hull girder in waves, and also an experimental model used for the validations. Their numerical model is based on the non-linear strip theory for the hydrodynamic problem, while the structural part was considered as two rigid bodies connected to each other by a non-linear rotational spring. The numerical model was employed to assess the severity of the collapse under large single wave loads.

Derbanne et al. [13] presented a simplified method to investigate the dynamic hull girder response by considering the non-linear effect of hull girder ultimate strength. The numerical model is the well-known single degree of freedom vibration model, which can take different moment-curvature relation curves and different hydrodynamic loading sequences. From the hydrodynamic point of view, the model deals with realistic loading scenarios, including the still water bending moment, the wave bending moment, and a slamming load. Derbanne et al. introduced the dynamic ultimate capacity factor, as the maximum allowable linear whipping response equivalent to a non-linear dynamic response reaching the failure point. It was shown that the dynamic ultimate capacity factor is highly dependent on the non-linear model of the hull girder behavior. However, it is always greater than unity, meaning that the linear dynamic response of the hull girder can exceed the quasi-static ultimate capacity without reaching the failure point. In conclusion, Derbanne et al. point out the necessity of using real loading sequences and show that simple loading scenarios, as pure slamming impacts on still water, will overestimate the dynamic ultimate capacity factor.

Yamada [14] investigated the possibility of using a commercial 3D FEM solver to simulate the dynamic elastic-plastic whipping response of a container ship due to slamming load. However, the full FE model is not considered as a free-floating body, as in a realistic scenario, but it is simply supported on the aft end. Also, the slamming load is balanced either by using the inertia relief method or using an opposite initial rotational velocity. These aspects are making the method developed by Yamada as being far from real physical phenomena. Henceforth, the methodology proposed by Yamada will not yield correct information on the dynamic elastic-plastic response of ships.

Going back in the literature, it can be seen that some researchers have questioned the validity of comparing the conventional hull girder ultimate capacity with the whipping induced extreme bending moment. Fewer have pointed the inconsistency in considering the ship's structural response as linear and elastic in the hydro-elastic whipping load on the one hand, and as non-linear and elastic-plastic in the ultimate strength capacity on the other hand. To the authors' point of view, it is essential to develop a non-linear whipping model that considers geometric non-linearities as well as material non-linearities. This aspect is essential for the design of modern ships, and it has never been addressed in a satisfactory way. Therefore, this research work proposes a new computational model for analyzing the non-linear whipping response in head waves. Needless to say, whipping is by nature always "non-linear" from a hydrodynamic point of view, the distinction between "linear" and "non-linear" in the forthcoming chapters pertains to the structural model.

STRUCTURAL MODEL

Modern container ships are of truly gigantic size, but for the purpose of dynamic analysis, such ships can be very well represented as a thin beam. It is essential to take into account that in real cases, only a very limited extent of the structure collapses [15, 16]. The reason for this is that in the real structures, there are heterogeneous loads and strengths, and one "frame spacing" tends to fail while the others do not. Hence the collapse area associated with a "weak frame" in the hull girder can be concentrated at a node of the beam model. In this research work, the hull girder is modeled as two non-uniform Timoshenko beams, connected with a non-linear hinge, as depicted in Fig. 1.

The non-linear hinge can be modeled as two coincident nodes, where the additional rotation due to the collapse is represented as the relative rotation between the two rotational degrees of freedom: one associated with the left part (or aft part)

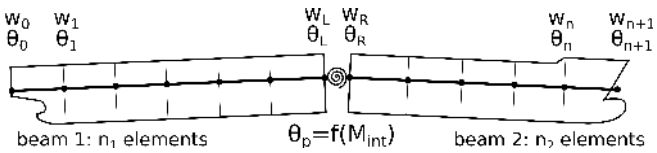

FIGURE 1: HULL GIRDER MODEL INCLUDING A NON-LINEAR HINGE

of the model, one associated with the right part (fore part) of the model. The behavior of this hinge is described by the non-linear relation between the internal bending moment and the relative rotation angle, i.e., the well-known moment-curvature curve used to describe the ultimate strength of a ship section. It should be noted that the non-linear hinge induces "stiff" relationships between degrees of freedom in the model, and therefore, in order to enforce the equality/inequality of degrees of freedom (DOF) of the coincident nodes Lagrange multipliers are used.

Usually, when performing the ultimate strength evaluation of a ship's section of length L within a 3D NL-FEA software, the hull girder's section is subjected to pure bending moment: M_{ext}. As a consequence, the structure will respond with the rotations of the aft- and fore-end sections denoted as θ_{aft}, and θ_{fore}, as depicted in Fig. 2. If one directly evaluates the relative rotation given by the 3D NL-FEA model $\theta = \theta_{aft} - \theta_{fore}$, then this rotation will contain the linear part, which is proportional to the extent of the section L, and the non-linear part which can be considered to be independent of L. The linear elastic rotation due to internal moment M_{int} on extent L is given by: $\theta_{linear} = M_{int}L/EI$. But since the evaluation of the ultimate strength is performed under quasi-static conditions, the internal bending moment is equal to the external one: $M_{int} = M_{ext}$.

However, when the non-linear behavior is reduced to a node, the linear part of the stiffness is already included in the Timoshenko beam elements adjacent to the non-linear hinge, as shown in Fig. 2. Henceforth, in order to avoid the situation where the linear elastic behavior of the hull girder is taken twice into account (i.e., once in the beam elements, and once in the hinge itself) the linear part must be removed from the precomputed non-linear behavior, and the node should only include the non-linear part, as follows:

$$M = f_{NL}(\theta - \theta_{linear}) = f_{NL}(\theta_p) \tag{1}$$

This can be precomputed beforehand, to define a new hinge

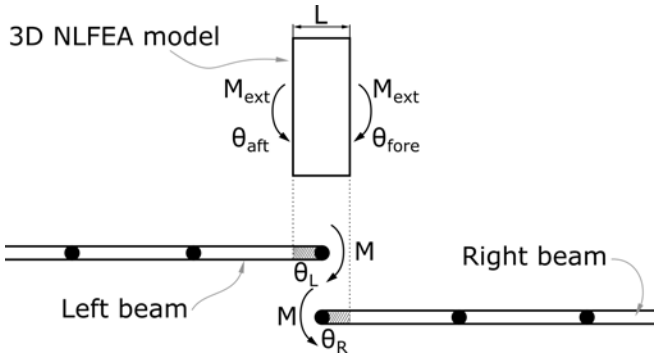

FIGURE 2: NON-LINEAR HINGE, NODAL ROTATIONS

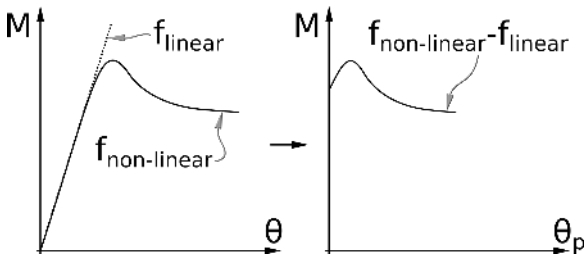

FIGURE 3: CHARACTERISTIC MODIFICATION FOR THE NON-LINEAR HINGE

characteristic $M_{int} = f_{NL}(\theta_p)$, as illustrated in Fig. 3. Where $\theta_p = \theta_L - \theta_R$ is the relative rotation angle of the non-linear hinge.

Non-uniform Timoshenko Beam Model

The hull girder is modeled as two non-uniform Timoshenko beams connected by a non-linear hinge, as Fig. 1 bears out. Each beam element is theoretically equivalent to a hull section; it is subjected to bending loads and taking into account the shearing deformations, according to the well-known elastic Timoshenko beam model [17]. For a two-dimensional beam element, each node has two degrees of freedom. In addition to the local DOF-s for the vertical displacement and rotation, which are defined at the neutral axis of the ship, one should include the global rigid-body DOF for the ship's surge motion, which is the axial translation along the x-axis and it is defined at the center of gravity.

The introduction of the rigid-body surge motion implies that all the structural matrices must be enhanced with one additional line and column. On the mass matrix, the first element of the diagonal will be M, which is the total mass of the ship. The remaining terms of the first line and first column are symmetrical and contain the coupling between surge and pitch motions. The coupling vector for surge-pitch motions has the following form for the left beam:

$$\boldsymbol{M}_1^{PS} = \begin{bmatrix} 0 & M_0 Z_0^{GC} & 0 & M_1 Z_1^{GC} & \dots & 0 & M_{n_1} Z_{n_1}^{GC} \end{bmatrix} \tag{2}$$

where $Z_j^{GC} = Z_G - Z_j^C$; Z_G denotes the z coordinate of ship's center of gravity; Z_j^C and M_j are the center of gravity and the mass, respectively, associated to node j.

Therefore, the structural matrices and the equation of motion for the structural part can be seen as:

$$\begin{bmatrix} M & \boldsymbol{M}_1^{PS} & \boldsymbol{M}_2^{PS} \\ \boldsymbol{M}_1^{PS} & \mathbf{m}_1 & \mathbf{0} \\ \boldsymbol{M}_2^{PS} & \mathbf{0} & \mathbf{m}_2 \end{bmatrix} \ddot{\boldsymbol{x}} + \begin{bmatrix} 0 & \mathbf{0} & \mathbf{0} \\ \mathbf{0} & \mathbf{b}_1 & \mathbf{0} \\ \mathbf{0} & \mathbf{0} & \mathbf{b}_2 \end{bmatrix} \dot{\boldsymbol{x}} + \begin{bmatrix} 0 & \mathbf{0} & \mathbf{0} \\ \mathbf{0} & \mathbf{c}_1 & \mathbf{0} \\ \mathbf{0} & \mathbf{0} & \mathbf{c}_2 \end{bmatrix} \boldsymbol{x} = \boldsymbol{F}_{ext} \tag{3}$$

$$\begin{aligned} \boldsymbol{x} &= \begin{bmatrix} u_x & w_0 & \theta_0 & w_1 & \theta_1 & \dots & w_{n+1} & \theta_{n+1} \end{bmatrix} \\ \boldsymbol{F}_{ext} &= \begin{bmatrix} F_x & F_0 & M_0 & F_1 & M_1 & \dots & F_{n+1} & M_{n+1} \end{bmatrix} \end{aligned} \tag{4}$$

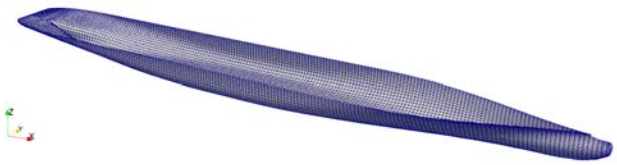

FIGURE 4: TYPICAL HYDRODYNAMIC MESH

where $\mathbf{m}_i$, $\mathbf{b}_i$, $\mathbf{c}_i$ are the mass, damping and stiffness matrices for the two beams $i = 1, 2$; $\boldsymbol{x}$ is the vector of displacements and $\dot{\boldsymbol{x}}$, $\ddot{\boldsymbol{x}}$ are the velocity and acceleration vectors, respectively; $\boldsymbol{F}_{ext}$ is the vector of external nodal forces.

The equation of motion presented in Eqn. 3 can be written in a more compact form as follows:

$$\mathbf{m}\ddot{\boldsymbol{x}}(t_{n+1}) + \mathbf{b}\dot{\boldsymbol{x}}(t_{n+1}) + \mathbf{c}\boldsymbol{x}(t_{n+1}) = \boldsymbol{F}_{ext}(t_{n+1}) \tag{5}$$

In the current context, a set of Lagrange multipliers are used to enforce the behavior of the non-linear hinge. The constraints to be imposed can be seen as: $\mathbf{B}_\wp \cdot \boldsymbol{x} = \boldsymbol{h}$. As consequence, one could include the boundary condition matrix $\mathbf{B}_\wp$, and its transpose in the enhanced stiffness matrix, $\tilde{\mathbf{c}}$, as follows:

$$\tilde{\mathbf{c}} = \begin{bmatrix} \mathbf{c} & \mathbf{B}_\wp^T \\ \mathbf{B}_\wp & \mathbf{0} \end{bmatrix} \quad , \quad \tilde{\boldsymbol{x}} = \begin{bmatrix} \boldsymbol{x} \\ \boldsymbol{\lambda} \end{bmatrix} \quad , \quad \tilde{\boldsymbol{F}}_{ext} = \begin{bmatrix} \boldsymbol{F}_{ext} \\ \boldsymbol{h} \end{bmatrix} \tag{6}$$

The enhanced force vector, $\tilde{\boldsymbol{F}}_{ext}$, embodies the constraints to be imposed to the system, denoted by the vector $\boldsymbol{h}$. On the other hand, the enhanced vector of displacements $\tilde{\boldsymbol{x}}$ includes the vector $\boldsymbol{\lambda}$, which can be seen as the internal load required to maintain the boundary conditions. As a consequence, the equation of motion will become a non-linear problem since the values of the enforced constraints are dependent on the internal loads and vice-versa. The numerical algorithm and the methodology developed to solve the elastoplastic problem of the non-linear hinge in order to follow the precomputed behavior will be discussed later in this paper.

HYDRO-ELASTIC MODEL

In order to solve the hydro-elastic problem, two meshes are necessary to model the geometry of the ship, namely the structural (presented in the foregoing section), and the hydrodynamic. The hydrodynamic one is used to solve the linear hydrodynamic Boundary Value Problem (BVP); a typical hydrodynamic mesh is depicted in Fig. 4.

Projection of the Shape Functions

The exact coupling between the finite beam element of the structure and the three-dimensional (3D) hydrodynamic model is

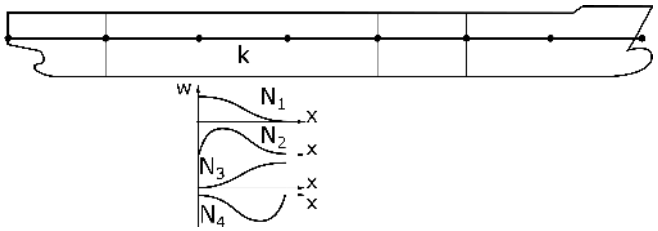

FIGURE 5: SHIP'S BEAM FINITE ELEMENT MODEL AND THE SHAPE FUNCTIONS

achieved by constructing the hydrodynamic BVP for each shape function of the finite elements, hence, for each degree of freedom, as proposed by Malenica [18].

For an isolated finite element k of length l the shape functions are illustrated in Fig. 5. The mode shapes are projected on the hydrodynamic mesh using the following methodology. For a mode j, the first step is to find all the hydrodynamic points which fall within the limits of an element k. Then, for every hydrodynamic point, P, the displacement vector, $\boldsymbol{h}^j$, is computed and can be seen as:

$$\boldsymbol{h}^j(P) = h_x^j(P)\vec{i} + h_y^j(P)\vec{j} + h_z^j(P)\vec{k} \tag{7}$$

where $h_x^j(P) = -N_{\theta_i}(x)\left(z(P) - z_{NA}^k\right)$, $h_y^j(P) = 0$, and $h_z^j(P) = N_{w_i}(x)$. N_{θ_i} and N_{w_i} are the classical Timoshenko beam shape functions for vertical deflection, and rotation, respectively. $\vec{i}$, $\vec{j}$, and $\vec{k}$ are the unit vectors in the x, y, and z direction, respectively. $z(P)$ is the vertical coordinate of the point P, and z_{NA}^k is the vertical position of the neutral axis for the element k. The procedure is repeated for all the shape functions, and for all the elements, yielding a total number of additional modes of $n_{mods} = 4 \cdot n_{elem}$. In addition to the modes represented by the shape function projection of each local DOF, it is necessary to define a global rigid-body mode which represents the surge motion.

Frequency Domain Coefficients

The hydrodynamic problem is considered within the usual assumptions of the potential flow. The total velocity potential of the fluid can be decomposed into the incident, diffracted, and the radiated component for every degree of freedom:

$$\varphi = \varphi_I + \varphi_D - i\omega \sum_{j=1}^{n_{mods}} \varphi_R^j \tag{8}$$

where φ_I is the incident potential, φ_D is the diffraction potential, and φ_R^j is the j-th radiation potential.

The diffraction and radiation velocity potentials are solved using the following BVP:

$$\begin{cases} \Delta\varphi = 0 & \text{, in the fluid} \\ -k\varphi + \dfrac{\partial\varphi}{\partial z} = 0 & \text{, z=0} \\ \dfrac{\partial\varphi}{\partial \boldsymbol{n}} = V_n & \text{, on } S_B \\ \lim\left[\sqrt{kR}\left(\dfrac{\partial\varphi}{\partial R} - ik\varphi\right)\right] = 0 & \text{, } R \to \infty \end{cases} \tag{9}$$

where V_n denotes the normal velocity which depends on the considered potential, S_B is the ship surface, R is the distance from the body, k is the wave number.

This complex BVP is solved numerically by using pulsating Green's source functions over the hydrodynamic mesh. Finally, the pressures components are calculated from the velocity potentials using the linearized Bernoulli equation, which leads to:

$$p_I = i\omega\rho\varphi_I \quad , \quad p_D = i\omega\rho\varphi_D \quad , \quad p_R^j = i\omega\rho\varphi_R^j \tag{10}$$

where p_I, p_D and p_R^j are the incident pressure, the diffraction pressure and the radiation pressure, respectively.

The hydrodynamic coefficients are obtained by an integration of the pressure over the wetted surface, by using the Gauss points distributed over the hydrodynamic mesh. Thus, the hydrodynamic coefficients can be expressed as:

$$\begin{gathered} F_I^j = \iint_{S_B} p_I \boldsymbol{h}^j \boldsymbol{n} \mathrm{d}S \qquad , \qquad F_D^j = \iint_{S_B} p_D \boldsymbol{h}^j \boldsymbol{n} \mathrm{d}S \\ A^{ij} + i\omega_e B^{ij} = \iint_{S_B} p_R^j \boldsymbol{h}^i \boldsymbol{n} \mathrm{d}S \end{gathered} \tag{11}$$

where: F_I is the incident wave force, F_D is the diffraction force, A is the hydrodynamic added mass, and B is the hydrodynamic damping.

Time Domain Simulations

Keeping in with the desire of predicting the structural response of a ship subjected to slamming loads, it is necessary, to perform the calculations in the time domain. Instead of solving directly the time-domain hydrodynamic problem, which can be extremely expensive, one well-known solution is to determine the hydrodynamic coefficients in time-domain by using the frequency-dependent added mass, damping, and diffraction forces. Henceforth, the equation of motion in time-domain resembles the usual equation, with the addition of the convolution integral over the past history for the velocity, as presented by Cummins [19]:

$$\begin{aligned} &(\mathbf{A}(\infty) + \mathbf{m})\ddot{\boldsymbol{x}}(t_{n+1}) + \mathbf{b}\dot{\boldsymbol{x}}(t_{n+1}) + \int_0^{t_{n+1}} \mathbf{K}(t_{n+1} - \tau)\dot{\boldsymbol{x}}(\tau)\mathrm{d}\tau \\ &\quad + (\mathbf{C} + \mathbf{c})\boldsymbol{x}(t_{n+1}) = \boldsymbol{F}(t_{n+1}) + \boldsymbol{Q}(t_{n+1}) \end{aligned} \tag{12}$$

where $\mathbf{A}(\infty)$ represents the infinite frequency added mass matrix, $\mathbf{C}$ is the restoring stiffness matrix, and $\mathbf{K}$ is the matrix of impulse response functions, which can be calculated from the frequency-dependent hydrodynamic damping coefficients [20]. $\mathbf{m}$, $\mathbf{b}$, and $\mathbf{c}$ are the structural matrices.

On the right side of equation Eqn. 12, the force vector $\boldsymbol{F}$ is composed of the diffraction force $\boldsymbol{F}_D$, incident wave excitation $\boldsymbol{F}_I$, the force due to gravity acceleration $\boldsymbol{F}_G$, and the force due to still water pressure $\boldsymbol{F}_{SW}$. $\boldsymbol{Q}$ is the vector of impulsive forces, i.e., slamming load. For the calculation of the incident and diffraction forces in time-domain, the complex RAO-s for the wave excitation calculated in the frequency domain are used. Aside from that, the time-domain forces are depending on the actual wave elevation around the body.

$$\boldsymbol{F}(t_{n+1}) = (\boldsymbol{F}_D + \boldsymbol{F}_I + \boldsymbol{F}_G + \boldsymbol{F}_{SW})(t_{n+1}) \tag{13}$$

HYDRO-ELASTOPLASTIC COUPLING

The first step towards solving the hydro-elastoplastic coupled problem is to upgrade the equations of motion presented in Eqn. 12 with a set of Lagrange multipliers. In the current context, the notation *tilde* ($\tilde{\square}$) has been adopted to differentiate the components whose size was increased with a specific number of Lagrange multipliers. The insertion of the Lagrange multipliers in the stiffness matrix, displacement vector, and the force vector is done as presented in Eqn. 6.

For the hydro-elastoplastic problem, three conditions have to be imposed: (i) the linear surge motion in order to handle the horizontal motions of the ship; (ii) the continuity of the vertical displacement field at the non-linear hinge, which can be seen as: $w_L - w_R = 0$; (iii) the discontinuity of the rotation field at the non–linear hinge, which can be seen as: $\theta_L - \theta_R = \theta_d = f(M_{int})$, and must follow the precomputed behavior. Henceforth, the vectors $\boldsymbol{h}$ and $\boldsymbol{\lambda}$, from Eqn. 6 can be seen as:

$$\boldsymbol{h} = \begin{bmatrix} u_{x_{lin}} & 0 & \theta_d \end{bmatrix}^T \quad , \quad \boldsymbol{\lambda} = \begin{bmatrix} F_x & SF_d & BM_d \end{bmatrix}^T \tag{14}$$

where SF_d represents the internal vertical shear force applied from the right node to the left node in order to enforce the continuity of the vertical displacement. BM_d represents the internal vertical bending moment between the degrees of freedom denoted θ_L and θ_R. It is worth mentioning that the internal vertical bending moment is defined as a non-linear function of the enforced discontinuity.

The equation of motion for the coupled hydro-elastoplastic problem becomes:

$$(\tilde{\mathbf{A}}(\infty)+\tilde{\mathbf{m}})\ddot{\tilde{\boldsymbol{x}}}(t_{n+1})+\tilde{\mathbf{b}}\dot{\tilde{\boldsymbol{x}}}(t_{n+1})+\int_0^{t_{n+1}}\tilde{\mathbf{K}}(t_{n+1}-\tau)\dot{\tilde{\boldsymbol{x}}}(\tau)\mathrm{d}\tau + (\tilde{\mathbf{C}}+\tilde{\mathbf{c}})\tilde{\boldsymbol{x}}(t_{n+1})=\tilde{\boldsymbol{F}}(t_{n+1})+\tilde{\boldsymbol{Q}}(t_{n+1}) \tag{15}$$

Numerical Time-Integration

It is well-know that when using implicit numerical schemes on constrained systems, some numerical errors in the form of numerical instabilities will occur even though the scheme is unconditionally stable for unconstrained systems [21, 22]. Henceforth, for ensuring numerical stability, the remedy is to add numerical damping for the high-frequencies in the time-stepping scheme. A popular scheme, widely used in the structural dynamics community for the numerical integration of linear and non-linear systems, but also in the commercial codes such as Abaqus or Ansys, is the Hilber-Hughes-Taylor (HHT) α-method [23].

According to [23], it is possible to include a specific amount of numerical damping in the system only by averaging elastic, inertial, and external forces between the current state of the system and the later one. The new form of the discretized equations of motions, presented in Eqn. 15, can be written as:

$$\begin{aligned}&(\tilde{\mathbf{A}}(\infty)+\tilde{\mathbf{m}})\ddot{\tilde{\boldsymbol{x}}}(t_{n+1})+(1+\alpha)\Big(\tilde{\mathbf{b}}\dot{\tilde{\boldsymbol{x}}}(t_{n+1})\\&+\int_0^{t_{n+1}}\tilde{\mathbf{K}}(t_{n+1}-\tau)\dot{\tilde{\boldsymbol{x}}}(\tau)\mathrm{d}\tau+(\tilde{\mathbf{C}}+\tilde{\mathbf{c}})\tilde{\boldsymbol{x}}(t_{n+1})\Big)\\&-\alpha\Big(\tilde{\mathbf{b}}\dot{\tilde{\boldsymbol{x}}}(t_n)+\int_0^{t_n}\tilde{\mathbf{K}}(t_n-\tau)\dot{\tilde{\boldsymbol{x}}}(\tau)\mathrm{d}\tau+(\tilde{\mathbf{C}}+\tilde{\mathbf{c}})\tilde{\boldsymbol{x}}(t_n)\Big)\\&=(1+\alpha)\Big(\tilde{\boldsymbol{F}}(t_{n+1})+\tilde{\boldsymbol{Q}}(t_{n+1})\Big)-\alpha\Big(\tilde{\boldsymbol{F}}(t_n)+\tilde{\boldsymbol{Q}}(t_n)\Big)\end{aligned} \tag{16}$$

where $\alpha\in[-1/2,0]$. In the current research work, a value of $\alpha=-0.05$ has been chosen for slight numerical damping. The smaller the value of α, the more damping is induced in the numerical solution.

The equation of motion can be easily solved by making use of the Newmark's equations [24], where the parameters γ and β are $1/2+\alpha$ and $1/4(1+\alpha)$, respectively. At first, the velocities and accelerations are rewritten with regards to the vector of displacements. Then, by making use of the linearization techniques, and after some rearrangement, the equation of motion (Eqn. 16) can be written in the following compact form, so as to solve for the displacements' increment:

$$\tilde{\mathbf{K}}_E\cdot\Delta\tilde{\boldsymbol{x}}=\tilde{\boldsymbol{F}}_E \tag{17}$$

where $\tilde{\mathbf{K}}_E$ and $\tilde{\boldsymbol{F}}_E$ are the effective stiffness matrix, and the effective force vector, respectively.

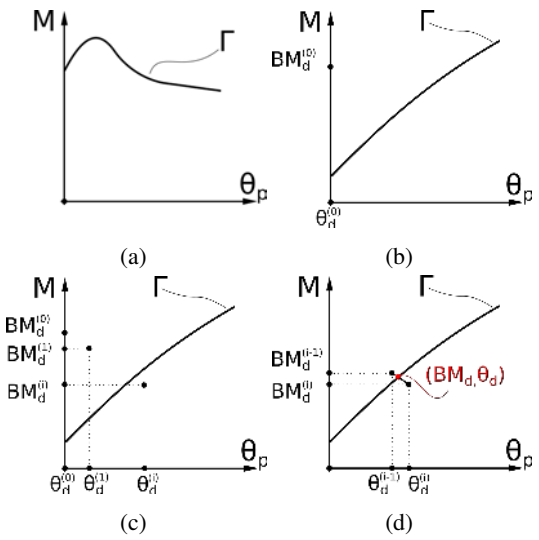

FIGURE 6: ITERATION STEPS FOR SOLVING THE NON-LINEAR PROBLEM (ZOOM ON CURVE Γ)

Numerical Algorithm

The system composed of two beams connected by a non-linear hinge represents a non-linear problem due to the direct dependency of the discontinuity of the rotations field, θ_d, and the internal bending moment at the discontinuity, BM_d. This problem can be solved iteratively in order to follow the precomputed behavior. As presented before, the non-linear relation between the plastic angle, θ_d, and the internal bending moment, BM_d, is described by the curve Γ, as Fig. 6a bears out.

Let the function f_{BM} as being the linear interpolation function over the curve Γ. At each event when the internal bending moment exceeds the yield limit, delimited by curve Γ, the iterative algorithm will search for a new discontinuity angle, higher than the previous one, to follow the precomputed behavior. Whenever the discontinuity is increased, the yield limit must be updated. Hence, this interpolation function will be used to determine the new yield limit for the cumulated discontinuity.

The search for the new plastic rotation angle starts when the internal bending moment, BM_d, computed at time instant t_n, exceeds the yield limit. At iteration (0) we have the point $\left(\theta_d^{(0)},BM_d^{(0)}\right)$ which is located above the curve Γ, as depicted in Fig. 6b. The discontinuity θ_d is increased at each iteration with an increment $\Delta\theta$, as follows:

$$\theta_d^{(i)}=\theta_d^{(i-1)}+\Delta\theta \tag{18}$$

After increasing the discontinuity the force vector is updated and the linear system is solved yielding a new solution, which can be represented by the point $\left(\theta_d^{(1)},BM_d^{(1)}\right)$. The iterative pro-

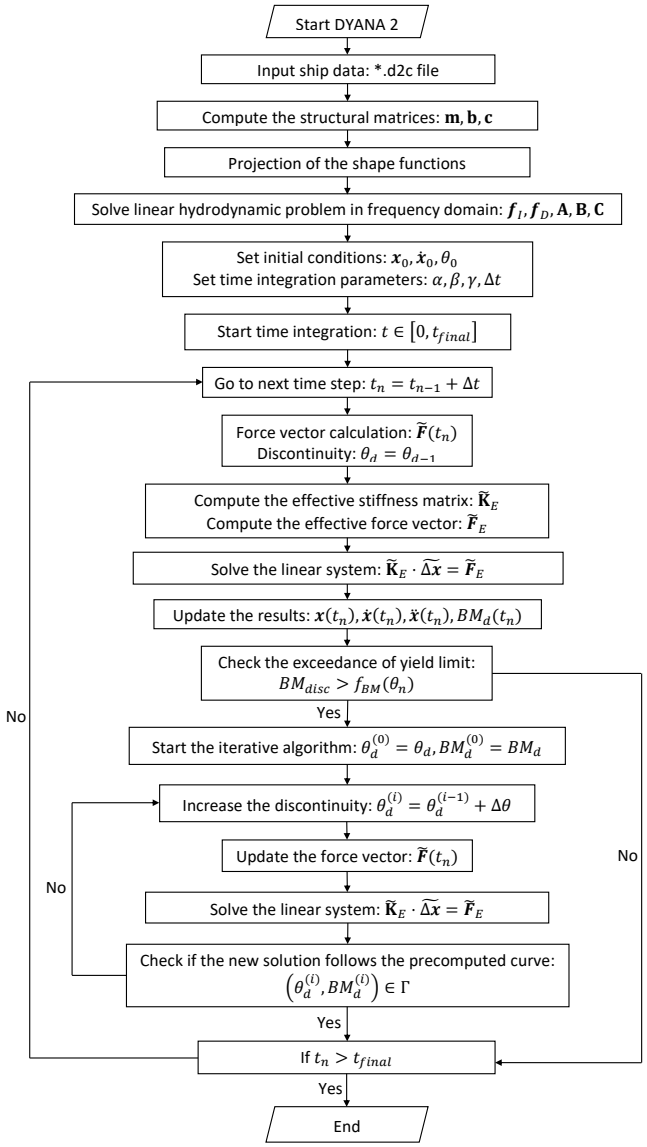

FIGURE 7: COMPUTATION SCHEME FOR SOLVING THE HYDRO-ELASTOPLASTIC PROBLEM

cedure continues until the new solution, $\left(\theta_d^{(i)}, BM_d^{(i)}\right)$, is situated below the yield limit, delimited by curve Γ, as shown in Fig. 6c.

The final solution is represented by the intersection point between the curve Γ and the curve delimited by the points $\left(\theta_d^{(i-1)}, BM_d^{(i-1)}\right)$ and $\left(\theta_d^{(i)}, BM_d^{(i)}\right)$, as Fig. 6d bears out.

One should keep in mind that slamming represents a fully non-linear phenomenon; hence, when coupling the structural problem with the hydrodynamic one, two iterative loops are necessary. The first one is used to compute the vector $Q(t)$, which depends on the instant displacements and velocities of the hull girder, and the former one is for the non-linear elastoplastic problem as depicted in Fig. 7. Within the current framework, a new software has been developed, named DYANA2, which solves the hydro-elastoplastic problem.

VERIFICATION AND VALIDATION

To the authors' knowledge, there are no studies, either numerical or experimental, on the hydro-elastoplastic response of ships subjected to slamming induced whipping response. This is mainly due to the complexities of the physical phenomena behind the two-way hydro-structure interaction. The non-linear behavior of the structural model and the nonlinearities within the hydrodynamic loading are posing certain difficulties to the mathematical model, but also for the computational cost. Because of the lack of experimental data, no proper "validation" is possible at this moment. As a consequence, only "verification" against other numerical codes is performed. Hence, the elastoplastic structural model and the hydro-elastic model separately are checked separately.

Elastoplastic Model

For the validation of the elastoplastic structural response, the current numerical model is compared with the results obtained from a commercial NL-FEA solver. Henceforth, by removing the hydrodynamic terms from the equation of motion (Eqn. 16), the problem resumes to a pure structural one.

With this in mind, the following collapse problem of a free-floating-like flexible steel tube can be defined. The structural model is depicted in Fig. 8. Along the length of the flexible tube, two different thicknesses are used; with a thinner tube in the middle, in order to create a "weak-frame" scenario. Moreover, the structural model is supported on a set of springs and dashpots in order to simulate the hydrodynamic damping and the restoring stiffness. The main particulars of the numerical model are as follows: length L=20m, tube diameter D=0.5m, tube thickness t_1=2mm, and t_2=1mm (for the collapse area), the springs stiffness is about 0.005N per unit length, and the dashpots coefficient is 0.3N/s/m; Young's modulus of 205.6 GPa, and Poisson ratio of 0.3. The mass density has been adjusted to ρ=10^{-6} t/mm^3 in order to obtain the frequencies for the first and second vertical modes of 0.68Hz, and 1.85Hz, respectively.

The non-linear structural behavior to be enforced on the collapse area is precomputed from a quasi-static analysis, using the NL-FEA solver, where both geometrical and material non-linearities are taken into account. The material model of choice is a bi-linear elastic-plastic model, including strain hardening with a slope of 1/1000.

The objective of the validation is to compare the structural response between the presented methodology, which is implemented in the software DYANA 2, with the results from ABAQUS. In ABAQUS, the precomputed behavior is enforced on the middle

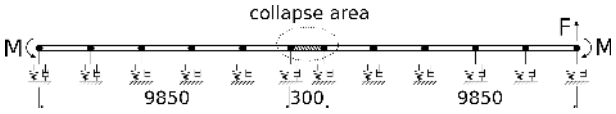

FIGURE 8: FREE-FLOATING-LIKE FLEXIBLE TUBE

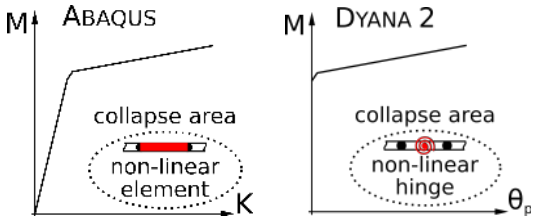

(a) (b)

FIGURE 9: DEFINITION OF THE NON-LINEAR BEHAVIOR

element, representing the collapse area, by making use of the non-linear generalized cross-section option [25]. The non-linear section response is assumed to be defined as a functional dependence of the bending moment in the function of curvature.

It is worth mentioning that in ABAQUS, the non-linear behavior is associated with an element of length L, as Fig. 9a bears out, and the non-linear sectional response includes the linear elastic part. In DYANA 2, the non-linear behavior contains only the plastic part since it is associated with a non-linear hinge, which is considered as a zero-length element, and the two adjacent elastic elements will give the elastic part, as Fig. 9b bears out. As a consequence, the FE model in ABAQUS has 11 elements, while the FE model in DYANA 2 has 12 elements.

The structure is subjected to a complex loading scenario composed of a constant component (still water bending moment alike), a low-frequency component (wave bending moment alike), and an impulsive load (slamming load alike). The time-variation of the imposed bending moment M, and imposed impulsive force F are depicted in Fig. 10. For the current example, a fixed time step of 0.01s has been used. It should be mentioned that the low-frequency bending moment component reaches about 90% of the structural capacity, and the collapse appears under the whipping induced bending moment.

For reasons related to the space limitation, only some of the results will be presented hereafter. In Figs. 11a, 11b, and 11c the comparison of the time histories for the plastic rotation angle, internal bending moment, and vertical displacement at the middle of collapse area, respectively, are presented; then, Fig. 11d illustrates curvature for the collapse area.

From Fig. 11, it can be seen than the whipping induced bending moment reaches the yield limit at the instant t=67s. With the further increase of the internal bending moment, permanent deformations are formed, and the plastic rotation angle θ_p shows

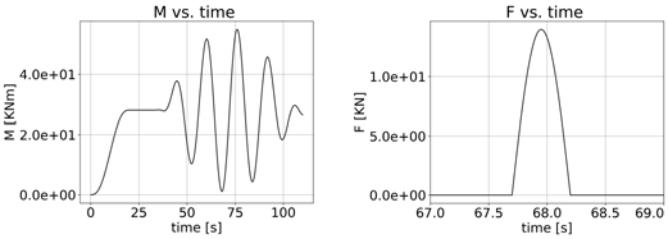

(a) (b)

FIGURE 10: TIME HISTORIES OF THE APPLIED LOADS

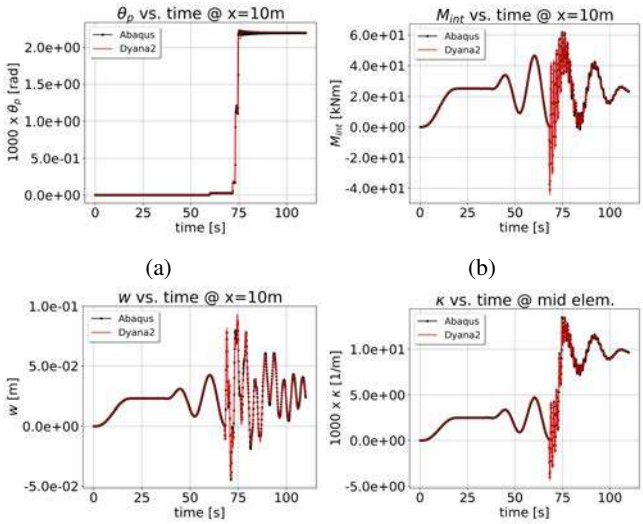

(a) (b)

(c) (d)

FIGURE 11: TIME HISTORIES AT THE COLLAPSE AREA

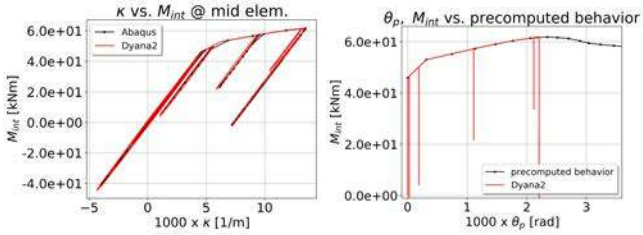

(a) (b)

FIGURE 12: COMPARISON OF THE NON-LINEAR BEHAVIOR

the severity of the collapse. Then, after t=80s, the structure starts to be unloaded, and its behavior will be elastic, but with a permanent deformation at the collapse area.

The capability of the proposed model to follow the precomputed non-linear behavior is presented in Fig. 12b, which shows

an excellent agreement. Aside from that, the comparison of the internal moment (M_{int}) vs. curvature (κ) curve for the collapse area (i.e., mid element) is depicted in Fig. 12a, showing a good agreement between the non-linear element used in ABAQUS, and the non-linear hinge with two adjacent elastic elements implemented in DYANA 2.

Hydro-elastic Model

By imposing the continuity of the two beams (i.e., $\theta_p = 0$), the system behaves linear-elastic. For the validation and verification of the proposed methodology, the numerical results are compared with the ones obtained by making use of HOMER2, a software developed and maintained by Bureau Veritas [26].

In the current research work a large container ship with a length of 350m is defined and used to validate and verify the hydro-elastic coupling methodology. For the hydrodynamic computations, a number of 2500 panels per half-body have been used, while the ship's structure was modeled with 20 non-uniform Timoshenko beam elements. The ship is subjected to an irregular wave-train. Figure. 13a shows the time-histories for the vertical displacement amidship, while in Fig. 13b, the rotations are compared. Figure 13c presents the comparison of the internal bending moment at midship. Moreover, the deformed shape at the instant when the bending moment is maximum amidship is compared in Fig. 14.

The comparison of the presented results, obtained by two different methods, is excellent, showing the trustworthiness of the proposed methodology.

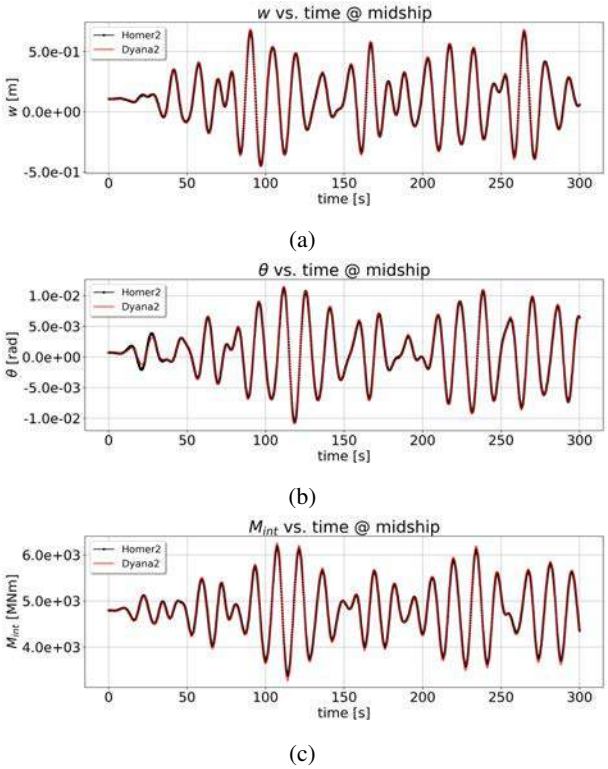

FIGURE 13: TIME HISTORIES FOR DIRECT TIME-DOMAIN ANALYSIS

HYDRO-ELASTOPLASTIC APPLICATION EXAMPLE

To illustrate the applicability of the presented theory, a large container ship with a length of 350m is used. A realistic loading sequence composed of the still water component, wave component and impulsive load is used in this study. The equivalent design wave is chosen in such a way that it targets the maximum hogging bending moment at t=0s. The sum of the still water and the wave-induced bending moment are reaching about 90% of the structural capacity, and the plastic deformations are appearing under slamming induced whipping response. It is worth mentioning that for the current example, a fixed time step of 0.1s has been used, resulting in a computational time of only two seconds for each second in real-time.

The time history for the internal bending moment amidship is presented in Fig. 15a. In Fig. 15b, it can be seen that the deformed shape at instant when internal bending moment is maximum amidship is affected by permanent plastic plastic deformations. As Fig. 15a bears out, at time instant t=-13s, the first slamming event appears, and the hull girder starts to vibrate. Then, the slamming induced whipping vibrations will increase the maximum hogging bending moment. A detail of the corresponding linear and non-linear bending moments are illustrated in Fig. 16a. It can be seen that when the non-linear structural behavior is considered, the maximum hogging bending moment is reduced. At instant t=-3s, the yield limit is exceeded, and the structure starts to behave nonlinearly. Hence, the relative rotation angle increases, as depicted in Fig. 16b.

The drop in the bending moment shows that it is possible to have a loading scenario leading to structural collapse if a linear dynamic response is considered, but it might lead to some plastic deformations without reaching the structural collapse if the non-linear dynamic response is considered.

With regard to this, Derbanne et al. [13] introduced the dynamic ultimate capacity factor in order to compare the results of conventional linear dynamic models to the non-linear ultimate capacity. The dynamic ultimate capacity factors will be further investigated with the proposed hydro-elastoplastic structural model.

CONCLUSION

This paper describes a new approach developed to compute the non-linear whipping response using hydro-elastoplastic coupling. Within the current approach, the structure is modeled as

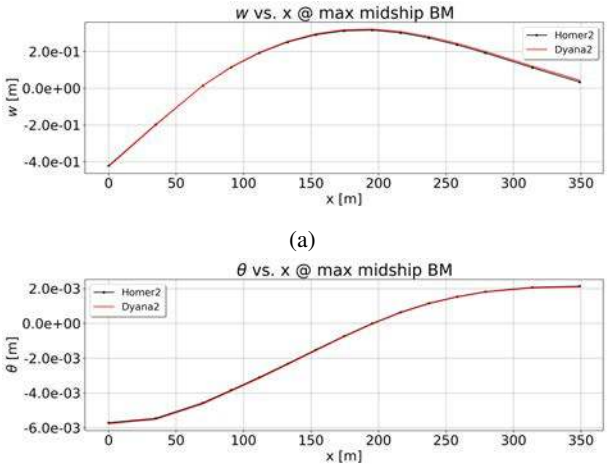

FIGURE 14: DEFORMED SHAPE AT INSTANT WHEN INTERNAL BENDING MOMENT IS MAXIMUM AMIDSHIP

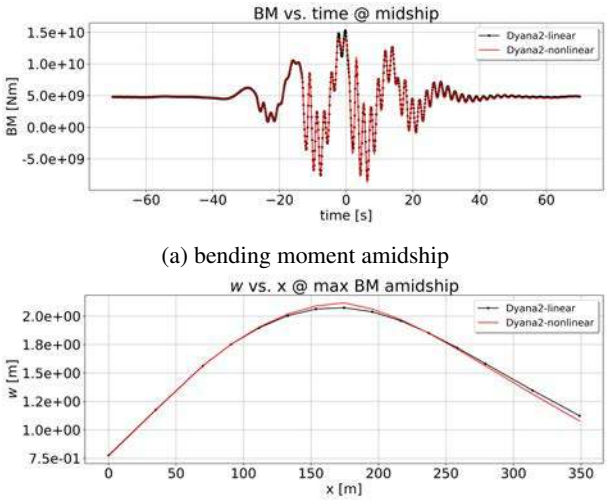

FIGURE 15: COMPARISON BETWEEN LINEAR AND NON-LINEAR WHIPPING

two non-uniform Timoshenko beams connected by a non-linear hinge. The exact coupling between the structural model and the 3D hydrodynamic model is achieved by constructing the hydrodynamic BVP for each shape function of the finite elements. After solving the complex BVP-s for a range of frequencies, the hydrodynamic coefficients in terms of added mass, wave damping, and wave excitation are determined. Then, the time-domain simulation is performed by making use of the frequency-dependent hydrodynamic coefficients, and by computing the radiation force from the memory-response functions and the history of velocities. Finally, the hydro-elastoplastic problem is solved within an iterative manner in order to follow the precomputed behavior of the non-linear hinge.

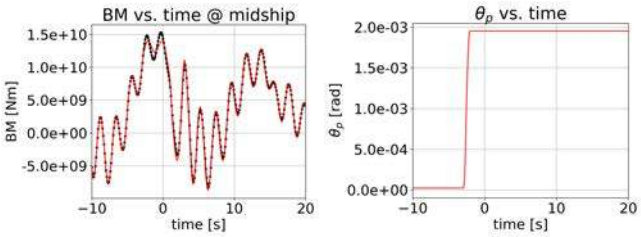

(a) bending moment amidship (b) permanent rotation angle

FIGURE 16: COMPARISON BETWEEN LINEAR AND NON-LINEAR WHIPPING

The performance of the proposed model is firstly validated regarding the elastoplasticity of a simple structure composed of a flexible tube supported on a set of springs and dashpots. The non-linear hinge model allows for fast computation and shows very good accuracy when compared with the non-linear elastic-plastic finite element analysis results. Then, the hydro-elastic coupling procedure, based on the shape function approach, is validated with the results obtained using a well-known hydro-structure interaction software, based on the generalized modes approach. The main advantage of the shape function approach is that the entire base of degrees of freedom is used, allowing for the inclusion of the non-linear structural response. The hydro-elastoplastic model allows for a fast computation of the non-linear whipping response (i.e., considering the non-linear structural behavior) on realistic scenarios such as equivalent design waves, or design sea states. Comparing to a strongly coupled CFD-FEM approach, where both domains should be considered non-linear, the computational time of the proposed approach is significantly reduced: from days to minutes. Aside from that, the non-linear hinge model can account for the cumulative permanent plastic deformation; the memory effect when the hull girder is subjected to several critical load scenarios.

Finally, the newly developed numerical method is applied on an ultra-large container ship in order to illustrate the differences between the linear whipping response (i.e., obtained using a linear elastic structural behavior), and the non-linear whipping response (i.e., using a non-linear structural behavior.) This final aspect will be further investigated in a parametric manner, with regards to the non-linear behavior curves, and to different realistic loading scenarios, as proposed by [13].

ACKNOWLEDGMENT

The present research work was undertaken at Ecole Centrale de Nantes, France, as a part of the Ph.D. thesis on the analysis

of whipping effects over the hull girder's ultimate strength. The first author is pleased to acknowledge the funding and support of Bureau Veritas via BV-ECN cooperation.

REFERENCES

[1] Bishop, R. E., and Price, W. G., 1979. *Hydroelasticity of ships*. Cambridge University Press.

[2] Chen, X.-j., Wu, Y.-s., Cui, W.-c., and Jensen, J. J., 2006. "Review of hydroelasticity theories for global response of marine structures". *Ocean Engineering,* ***33***(3-4), pp. 439–457.

[3] Hirdaris, S., and Temarel, P., 2009. "Hydroelasticity of ships: recent advances and future trends". *Proceedings of the Institution of Mechanical Engineers, Part M: Journal of Engineering for the Maritime Environment,* ***223***(3), pp. 305–330.

[4] Ergin, A., Alley, E., Brandt, A., Drummen, I., Hermundstad, O. A., Huh, Y.-C., Ivaldi, A., Liu, J., Malenica, Š., el Moctar, B. O., et al., 2018. "Issc committee ii. 2–dynamic response". In Proceedings of the 20th International Ship and Offshore Structures Congress (ISSC 2018), IOS Press.

[5] Tuitman, J., and Malenica, Š., 2009. "Fully coupled seakeeping, slamming, and whipping calculations". *Proceedings of the Institution of Mechanical Engineers, Part M: Journal of Engineering for the Maritime Environment,* ***223***(3), pp. 439–456.

[6] Kim, K.-H., Bang, J.-S., Kim, J.-H., Kim, Y., Kim, S.-J., and Kim, Y., 2013. "Fully coupled bem-fem analysis for ship hydroelasticity in waves". *Marine Structures,* ***33***, pp. 71–99.

[7] Seng, S., 2012. "Slamming and whipping analysis of ships". PhD thesis, DTU Mechanical Engineering.

[8] Takami, T., and Iijima, K., 2019. "Numerical investigation into combined global and local hydroelastic response in a large container ship based on two-way coupled cfd and fea". *Journal of Marine Science and Technology*, pp. 1–17.

[9] Branch, M. A. I., 2008. Report on the investigation of the structural failure of msc napoli, english channel on 18 january 2007. Tech. rep., Marine Accident Investigation Branch.

[10] ClassNK, 2014. Investigation report on structural safety of large container ships. Tech. rep., ClassNK.

[11] Lehmann, E., 2006. "Discussion on report of committee iii. 1: ultimate strength". *Proceedings of 16th ISSC, Southampton, UK, 2006,* ***3***, pp. 121–131.

[12] Iijima, K., Kimura, K., Xu, W., and Fujikubo, M., 2011. "Hydroelasto-plasticity approach to predicting the post-ultimate strength behavior of a ship's hull girder in waves". *Journal of marine science and technology,* ***16***(4), pp. 379–389.

[13] Derbanne, Q., de Lauzon, J., Bigot, F., and Malenica, S., 2016. "Investigations of the dynamic ultimate strength of a ship's hull girder during whipping". *Proceedings of PRADS2016,* ***4***, p. 8th.

[14] Yamada, Y., 2019. "Approach to simulate dynamic elasto-plastic whipping response of global hull girder of a large container ship due to slamming load". In The 29th International Ocean and Polar Engineering Conference, International Society of Offshore and Polar Engineers.

[15] Matsumoto, T., Shigemi, T., Kidogawa, M., Ishibashi, K., and Sugimoto, K., 2016. "Examination of effect of lateral loads on the hull girder ultimate strength of large container ships". In ASME 2016 35th International Conference on Ocean, Offshore and Arctic Engineering, American Society of Mechanical Engineers.

[16] Jagite, G., Le Sourne, H., Cartraud, P., Bigot, F., Derbanne, Q., and Malenica, Š., 2019. "Examination of the dynamic effects on the hull girder ultimate strength of ultra large container ships". In Trends in the Analysis and Design of Marine Structures: Proceedings of the 7th International Conference on Marine Structures (MARSTRUCT 2019, Dubrovnik, Croatia, 6-8 May 2019), CRC Press, p. 137.

[17] Timoshenko, S., and Goodier, J., 1951. Theory of elasticity 2nd edition.

[18] Malenica, Š., 1998. "Hydroelastic coupling of beam structural model with 3d hydrodynamic model". In 2nd Int. Conf. on Hydroelasticity.

[19] Cummins, W., 1962. The impulse response function and ship motions. Tech. rep., David Taylor Model Basin Washington DC.

[20] Ogilvie, T. F., 1964. "Recent progress toward the understanding and prediction of ship motions". In 5th ONR Symp. on Naval Hydrodynamics.

[21] Cardona, A., and Géradin, M., 2001. *Flexible multibody dynamics: a finite element approach*. John Wiley.

[22] Géradin, M., and Rixen, D. J., 2014. *Mechanical vibrations: theory and application to structural dynamics*. John Wiley & Sons.

[23] Hilber, H. M., Hughes, T. J., and Taylor, R. L., 1977. "Improved numerical dissipation for time integration algorithms in structural dynamics". *Earthquake Engineering & Structural Dynamics,* ***5***(3), pp. 283–292.

[24] Newmark, N. M., et al., 1959. "A method of computation for structural dynamics". *Journal of the Engineering Mechanics Division,* ***85***(3), pp. 67–94.

[25] ABAQUS, 2017. Dassault Systemes Simulia Corp, Johnston, RI, USA.

[26] Derbanne, Q., Malenica, Š., Tuitman, J., Bigot, F., and Chen, X., 2010. "Validation of the global hydroelastic model for springing & whipping of ships". In 11th International Symposium on Practical Design of Ships and Other Floating Structures, Rio de Janeiro, 331-340.